Photoelectrochemical complexes for solar energy conversion that chemically and autonomously regenerate

Moon-Ho Ham[1†], Jong Hyun Choi[2†], Ardemis A. Boghossian[1†], Esther S. Jeng[1], Rachel A. Graff[1], Daniel A. Heller[1], Alice C. Chang[1], Aidas Mattis[3], Timothy H. Bayburt[3], Yelena V. Grinkova[3], Adam S. Zeiger[4], Krystyn J. Van Vliet[4], Erik K. Hobbie[5], Stephen G. Sligar[3], Colin A. Wraight[3] and Michael S. Strano[1*]

Naturally occurring photosynthetic systems use elaborate pathways of self-repair to limit the impact of photo-damage. Here, we demonstrate a complex consisting of two recombinant proteins, phospholipids and a carbon nanotube that mimics this process. The components self-assemble into a configuration in which an array of lipid bilayers aggregate on the surface of the carbon nanotube, creating a platform for the attachment of light-converting proteins. The system can disassemble upon the addition of a surfactant and reassemble upon its removal over an indefinite number of cycles. The assembly is thermodynamically metastable and can only transition reversibly if the rate of surfactant removal exceeds a threshold value. Only in the assembled state do the complexes exhibit photoelectrochemical activity. We demonstrate a regeneration cycle that uses surfactant to switch between assembled and disassembled states, resulting in an increased photoconversion efficiency of more than 300% over 168 hours and an indefinite extension of the system lifetime.

Self-repair processes in plants, algae and photosynthetic bacteria use molecular recognition and metastable thermodynamic states to make protein complexes that can be continually repaired by partial disassembly and reassembly with new components, initiated by chemical signals alone. For example, the repair of protein D1 in photosystem II (PS II) when photo-damaged is initiated by photoinactivation of the protein induced by both the acceptor side and the donor side. This results in peptide bond scissions that alter protein conformation and drive dissociation of the damaged complex from the large PS II assemblies embedded within membrane stacks inside the chloroplast of a plant cell[1]. The separated complex diffuses laterally from within the stacks of membranes and out towards the outer membrane regions, where it disassembles into peripheral light-harvesting complex II (LHC II) and a PS II core complex[2]. The damaged D1 component of the PS II core is then fully degraded and the depleted complex equilibrates with newly biosynthesized D1 protein, resulting in the self-assembly of a tightly bound, repaired complex. The repaired complex returns to within the membrane stacks, where it re-docks with the extended light-harvesting systems inside the membranes, thus completing the repair cycle[1]. Central to this self-repair process are molecular recognition of the components and thermodynamic metastability, which allow the system to reversibly transition between kinetically trapped and disassembled states. In this work, we extend these concepts to develop the first synthetic photoelectrochemical complex capable of mimicking key elements of this self-repair cycle.

Results and discussion

To develop such a complex, we examined the use of phospholipid-based light-harvesting nanostructures. Phospholipids have been used previously to disperse single- and multiwalled carbon nanotubes[3], and the dialysis of phospholipids such as 1,2-dimyristoyl-sn-glycero-3-phosphocholine (DMPC) in the presence of an amphipathic apolipoprotein (membrane scaffold protein; MSP) creates a lipid bilayer nanodisc (ND) approximately 10 nm in diameter and 5 nm in height, as shown previously[4]. We find that such discs assemble onto a single-walled carbon nanotube (SWNT) so that the diameter is parallel to the nanotube, creating a platform for attaching membrane proteins (Fig. 1).

One protein of interest for photoelectrochemical conversion is the photosynthetic reaction centre (RC) isolated from the purple bacterium *Rhodobacter sphaeroides*[5]. This bacterial reaction centre comprises a protein complex composed of four bacteriochlorophylls (Bchls), two bacteriopheophytins (Bphes), and primary and secondary ubiquinones (Q_A and Q_B). Upon photoabsorption, the complex acts as a photoconverter, shuttling the formed exciton to the Bchl dimer (called the primary donor, P), where charge is separated, with the hole remaining (P^+) and the electron transferred to the Q_B site on the other side of the reaction centre through an electron transfer reaction[6]. Incorporation of the reaction centre into the nanodisc locates the hole injection site (P^+) so that it is directly facing the carbon nanotube, which may then act as a molecular hole conducting wire.

We find that this ordered assembly of lipids, membrane scaffold protein, nanodisc and SWNT forms spontaneously when a sodium

[1]Department of Chemical Engineering, Massachusetts Institute of Technology, Cambridge, Massachusetts 02139, USA, [2]School of Mechanical Engineering, Purdue University, Birck Nanotechnology Center, Bindley Bioscience Center, West Lafayette, Indiana 47907, USA, [3]Department of Biochemistry, University of Illinois at Urbana-Champaign, Urbana, Illinois 61801, USA, [4]Department of Materials Science and Engineering, Massachusetts Institute of Technology, Cambridge, Massachusetts 02139, USA, [5]Polymers Division, National Institute of Standards and Technology, Gaithersburg, Maryland 20899, USA; [†]These authors contributed equally to this work. *e-mail: strano@mit.edu
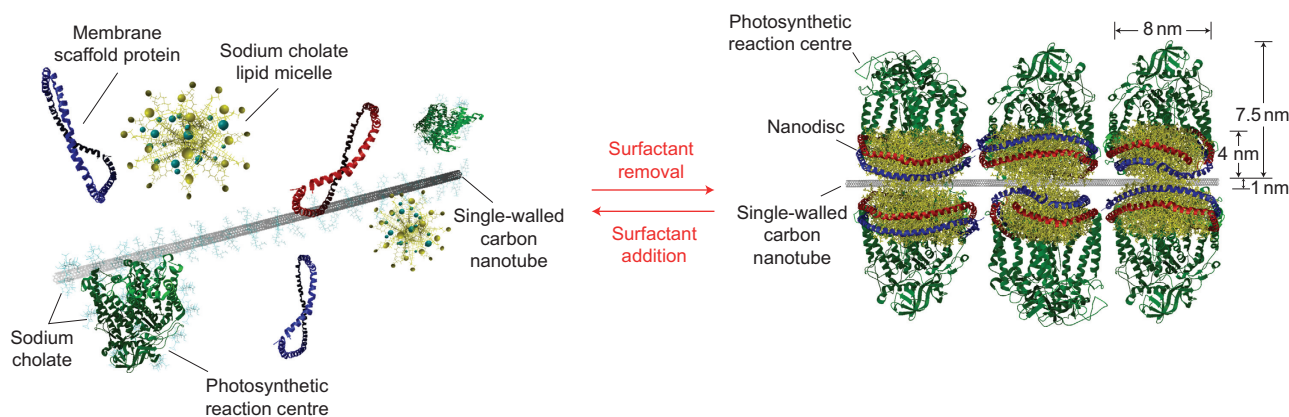
Figure 1 | Schematic of self-assembled photoelectrochemical complexes. The self-assembly process involves carbon nanotubes and photosynthetic reaction centres and occurs upon surfactant (sodium cholate) removal. Membrane dialysis induces spontaneous self-assembly of DMPC and membrane scaffold proteins to form nanodiscs, which reconstitute the reaction centres while suspending nanotubes in aqueous solution. The resulting, highly ordered complex is shown in the right-hand panel. Addition of sodium cholate completely decomposes the complexes back into the individual components in the initial condition (left-hand panel).

cholate-suspended mixture of each of the components is dialysed to remove the surfactant. Control experiments (Supplementary Fig. S7) confirm that all components are necessary for the structure to form. The complexes are broken apart upon the re-introduction of 2 wt% sodium cholate in a cycle that can be repeated indefinitely with no irreversible degradation of the photoelectrochemical properties of the assembled state, as described below.

We confirmed the parallel arrangement of the nanodiscs along the nanotube surface using atomic force microscopy (AFM) and small-angle neutron scattering (SANS). A typical AFM image (Fig. 2a) reveals either free nanodisc stacks or nanodiscs assembled along the nanotube axis. The height profile (Fig. 2b) along the nanotube, which indicates a height of 8 ± 0.4 nm, is consistent with a bilayer stack on either side of the nanotube. The specific orientation of the discs is confirmed by SANS (Supplementary Section S1). Figure 2c,d shows the scattering intensity versus reciprocal lattice vector for a nanodisc (red, Fig. 2c) and ND–SWNT (red, Fig. 2d), described by the best fit model of an isotropic suspension of monodisperse discs with diameters of 8 nm and heights of 4 nm (blue, Fig. 2c) and a series of parallel discs in a linear arrangement (black, Fig. 2d), respectively. The parallel arrangement leads to a maximum in scattering at $q = 2\pi/(2R)$, where R is the radius. In contrast, the blue curve in Fig. 2d compares the same data with that of an isotropic dispersion, highlighting the difference. These experimental results confirm the disc dimensions of 8 nm (diameter) and 4 nm (height) and the particular parallel stacking

arrangement along the nanotube. This arrangement allows for membrane proteins to orientate orthogonally to the nanotube surface. Specifically, this arrangement conveniently projects the hole injection site of the reaction centre in close proximity to the nanotube surface, as depicted in Fig. 1.

We used density gradient centrifugation to specifically isolate the complexes from background components and further verify their structure[7]. The mixtures were added to a 5-ml stop layer of 60 v/v% iodixanol and, subsequently, five density gradient layers of 50, 40, 30, 20 and 10 v/v% iodixanol/water solutions (1 ml each) were serially added in a centrifuge tube. Assembled ND–SWNT, RC–ND and free lipids (that is, no membrane scaffold protein) were also examined as controls. After centrifugation at 30,000 r.p.m. for 7 h, each sample in the tube was fractionated in twenty 250-μl increments along the density gradient into a 96-well plate. A fluorescence well plate reader was used to track the fluorescent emission of a lipid-soluble Laurdan dye[8], which indicated the presence of hydrophobic phases (Fig. 3a). Free lipid is significantly less dense than the hydrophobic nanodisc phases, all of which demonstrate a narrow peak near 1,052 kg m^{-3}, assigned as the lipid bilayer nanodisc. A homebuilt near-infrared (NIR) plate reader was used to track the fluorescence of the reaction centres themselves at 866 nm (Fig. 3b) and the fluorescence of the (9,1) SWNTs (Fig. 3c). When reaction centres are included in the mixture, they reconstitute into the nanodisc phase, as seen by the peak in the reaction centre photoluminescence (PL) centred at 1,050 kg m^{-3} in the absence of SWNTs (Fig. 3b). In
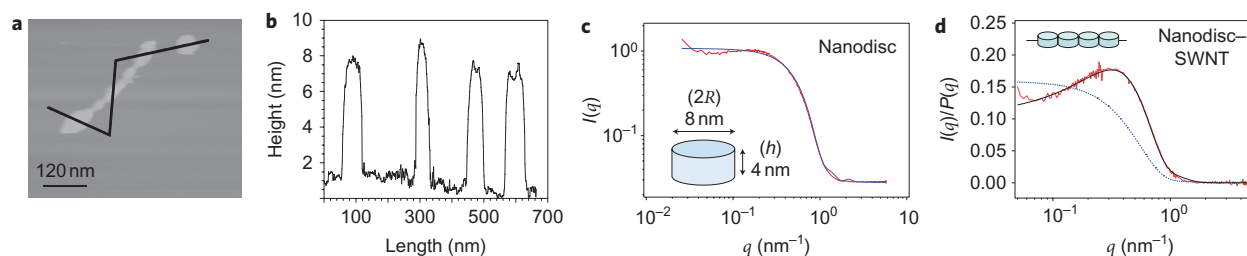

Figure 2 | Structural characterization of self-assembled photoelectrochemical complexes. a, AFM image showing a nanodisc and a ND–SWNT complex. **b**, Height profile showing that these nanostructures are ~8 nm in height. **c,d**, SANS measurements are shown in red for nanodisc (**c**) and ND–SWNT (**d**). The blue curve in **c** denotes a model fit to the form factor of an isotropic suspension of monodisperse discs, whereas the blue curve in **d** generates an unsatisfactory fit assuming isotropic disc form factor. The model fit in black (**d**) is in good agreement with the experimental data, assuming the factor for sequentially adsorbed discs, $q = 2\pi/(2R)$. These results confirm that nanodiscs have a diameter of ~8 nm and a height of 4 nm, and nanodiscs are stacked along the carbon nanotubes.
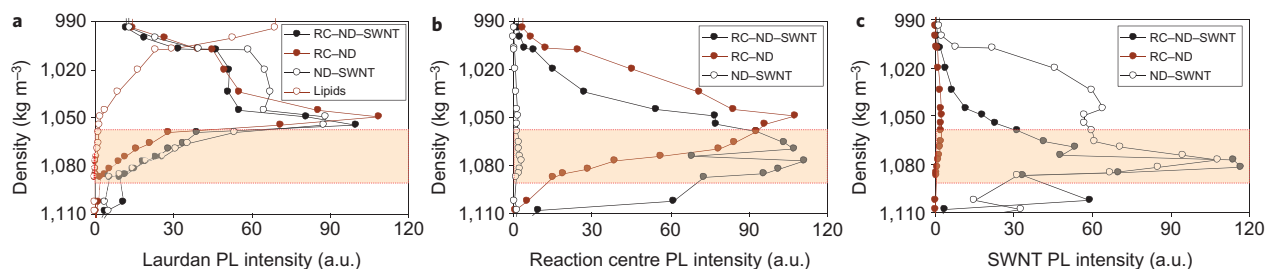
Figure 3 | Purification of self-assembled photoelectrochemical complexes. a–c, Fluorescence intensity distributions of the Laurdan dye (**a**), reaction centre (**b**) and SWNT (**c**) of the self-assembled complexes as a function of density after ultracentrifugation at 30,000 r.p.m. for 7 h. After ultracentrifugation, each sample in a centrifuge tube is fractionated in every 250 μl into a 96-well plate. The RC–ND and ND–SWNT samples are also examined as controls. Laurdan is used to identify the nanodisc distribution. Note that free lipids (that is, no membrane scaffold protein) are located only in the layer of density below 1,050 kg m^{-3}. The highlighted portions are collected for structural and photoelectrochemical characterizations.

contrast, when the reaction centres are added to the ND–SWNT complex, this peak shifts to 1,077 kg m^{-3}, precisely where the SWNTs show a maximum for the RC–ND–SWNT and the empty ND–SWNT systems in the gradient. Both these photoluminescences show overlapping peaks at 1,077 kg m^{-3} (Fig. 3c) where the reaction centre concentration is at a maximum. This analysis unambiguously confirms that the reaction centre is reconstituted in the nanodisc attached along the SWNT. Within the resolution of our experiment, the RC does not appear to alter the density of the ND–SWNT complex significantly, but the results confirm that the RC–ND–SWNT complex is stable and can be isolated free from constituent components.

A closer examination of the photoluminescence from the SWNT before and after nanodisc formation reveals that near armchair (n, n–1) species exhibit a large redshift (49 to 60 nm) of the emission wavelength (Fig. 4a). Before assembly, the SWNT fluorescence peak maxima are consistent for samples suspended in 2 wt% sodium cholate. Upon removal of the sodium cholate by dialysis for 30 min and subsequent formation of the RC–ND–SWNT structure described above, only the near armchair species in the mixture—(6,5), (7,6) and (8,7)—demonstrate this large photoluminescence redshift (Fig. 4b). A density separation analysis gives no indication of the occurrence of significant changes to the macromolecular structure for only these species. Because the chiral angle is so prominently recognized in spite of the wide variation in diameter and length among these three SWNT species, we hypothesize that the lipid bilayer in the nanodisc adsorbs such that the hydrocarbon chain of DMPC partially registers in a very specific manner with the graphene lattice, independent of the curvature of the SWNT sidewall. We note that the flexible hydrophobic chains are spaced such that they can align parallel to the unit vectors along the carbon atoms of the graphene lattice. Registration of hydrocarbon chains on SWNTs has been observed previously[4] for various surfactant molecules dissolved in water that are similar in size and properties to DMPC. However, in this work, the photoluminescence shift is only observed when the DMPC molecules are bound with the membrane scaffold protein and the entire nanodisc structure is formed. Because the DMPC head group is hydrophilic, we expect that only the two tails contribute significantly to the DMPC adsorption to SWNT. Therefore, molecular dynamics was used to energetically relax the DMPC molecule relative to the graphene using Hyperchem software, and the AMBER force field[9] was used to calculate the van der Waals energetic contribution for alignment to the graphene lattice of one of the two DMPC tails (13-carbon hydrophobic chain) (Supplementary Section S2). The van der Waals energy of the aligned chain is 1 kcal mol^{-1} more thermodynamically favourable than that of the random chain orientation with graphene. This result is in agreement with our energy-minimizing simulations, which indicate that the tails of the DMPC have a

tendency to align with the graphene lattice, regardless of the initial DMPC conformation and orientation (Fig. 4d). This favourable alignment is consistent with a registry to the graphene lattice that is specific to the species of nanotube.

One useful aspect of the SWNT photoluminescence shift is that it is only observed when the nanodisc phase forms at the nanotube sidewall, and molecules that denature or disrupt the phase decrease the photoluminescence redshift of the near armchair species back to values commensurate with other SWNT species (Fig. 4b). Nanotube suspensions added to other preparations such as membrane scaffold protein or lipid alone by dialysis do not cause the photoluminescence shift (Supplementary Fig. S7), illustrating that it is a useful optical probe of the assembly/disassembly processes.

Remarkably, the complex can be chemically disassembled by adding 2 wt% sodium cholate into the initial separated components and subsequently reassembled upon its dialysis from the system. Figure 4c shows the process of repeated assembly/disassembly cycles as monitored using the emission wavelength of the (6,5) nanotube. A dialysis flow chamber allowed for spectroscopic monitoring of a solution of 7 nM RC–ND–SWNT complex as a continuously supplied buffer was switched between surfactant-free and 2 wt% surfactant buffer. As the buffer was switched to surfactant-free media, the sodium cholate was dialysed from the sample, resulting in the assembly and subsequent PL redshift of the (6,5) nanotube as described above. Switching the buffer back to sodium cholate buffer caused the surfactant to diffuse back into the dialysis cell, disassembling the mixture into its starting components and blueshifting the emission. The process could be repeatedly cycled in this way with no loss in fidelity for at least five cycles over 15 h. Photoelectrochemical activity was also preserved, even after repeated assembly/disassembly in this manner, as shown below.

The reversible assembly/disassembly capabilities of such a specifically orientated complex have no analogue in any other synthetic photoelectrochemical structure, and we note that this is the first synthetic photoelectrochemical structure to mimic the dynamic equilibrium that forms the basis of natural self-repair. As discussed, this evolutionarily conserved self-repair process present in photosynthetic bacteria, algae and higher plants results in the replacement of damaged D1 proteins with a newly synthesized protein. In this self-repair process, the new protein is reassembled into a functional PS II using the same intermolecular forces that drive the self-assembly process demonstrated in the synthetic system in this work[1].

Both the natural complexes in living systems and the engineered complex introduced in this work can be considered metastable thermodynamic phases that are kinetically trapped into their functional state. To understand the dynamics behind the formation and disassembly process, we developed a kinetic model with 15 mechanistic
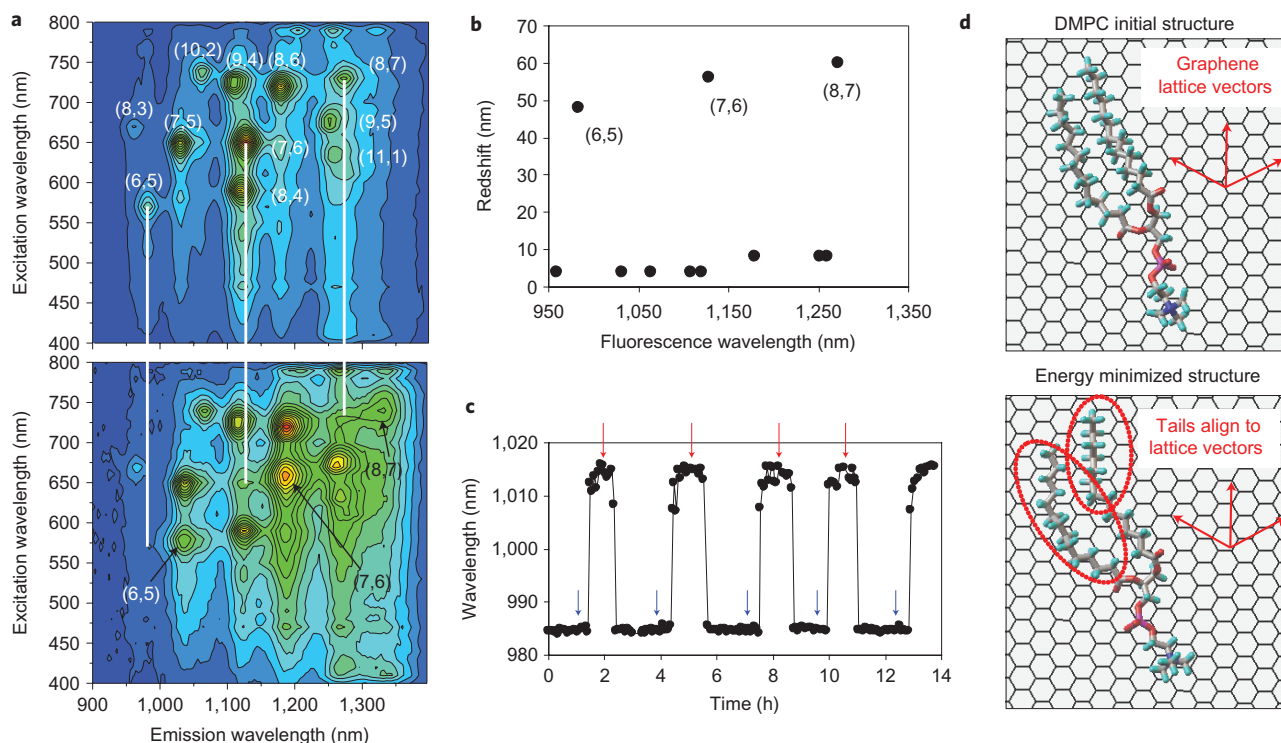
Figure 4 | Optical signatures of the assembled RC–ND–SWNT complex. a, Photoluminescence excitation contour of carbon nanotubes before (top) and after (bottom) dialysis. A few SWNT species demonstrate large fluorescence redshifts upon sodium cholate removal, which is interpreted as being indicative of nanodisc formation along the nanotube axis. **b**, SWNT fluorescence wavelength shifts upon nanodisc formation on SWNTs, identified from photoluminescence excitation spectra. Near armchair species (n, n–1) demonstrate large redshifts of 49–60 nm, whereas the spectral changes in other species are moderate. **c**, Plot of (6,5) photoluminescence maxima in a spectral window of 985–1,015 nm as a function of time during serial self-assembly and decomposition. Red arrows, addition of sodium cholate; blue arrows, removal of sodium cholate. **d**, Initial structure of DMPC (based on simulation), with the axis oriented at 25° relative to the graphene lattice vector (upper panel). The lower panel shows that the energy-minimized structure based on simulation has both DMPC tails aligned to the carbon atoms of the graphene lattice. Alignment of each tail contributes 1 kcal mol^{-1} of favourable van der Waals attraction compared to a randomly oriented tail.
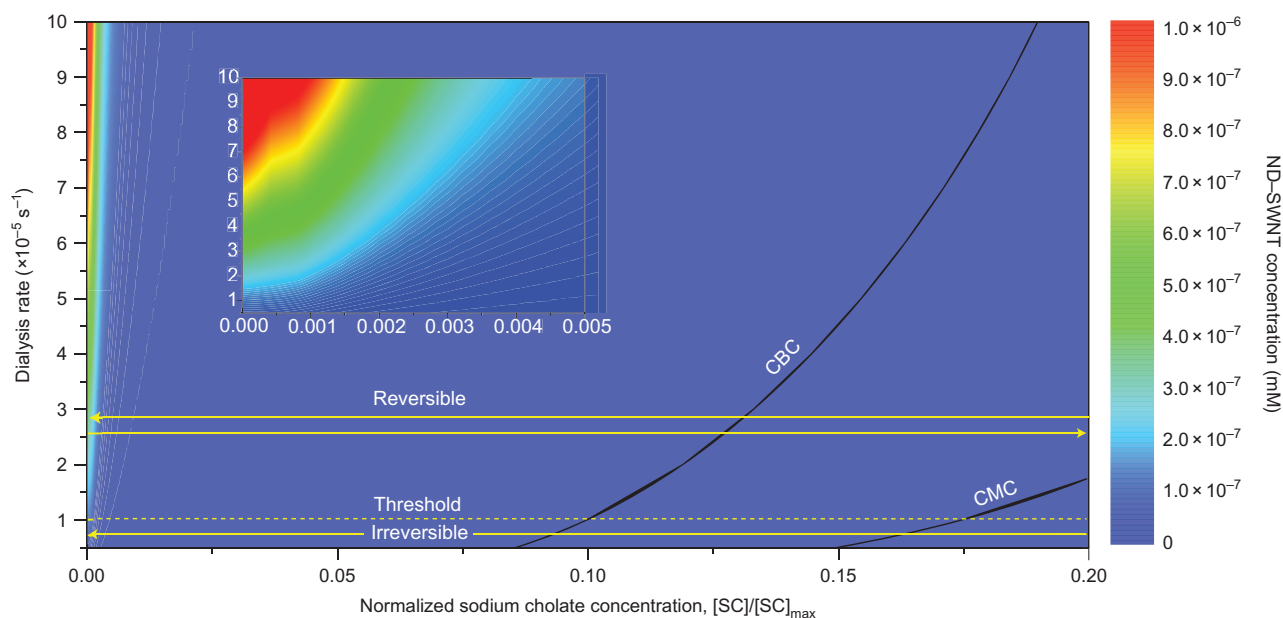

Figure 5 | Kinetic model illustrating ND–SWNT concentration throughout dialysis. Sodium cholate concentration refers to the total amount of free and micellar sodium cholate aggregates normalized with respect to the maximum concentration achieved at each dialysis rate. ND–SWNT complexes form below the critical micelle (CMC) and critical bilayer (CBC) concentrations, and concentration increases as the sample is dialysed to low sodium cholate concentrations at high rates, with a minimum threshold rate of 1.0×10^{-5} s^{-1}.
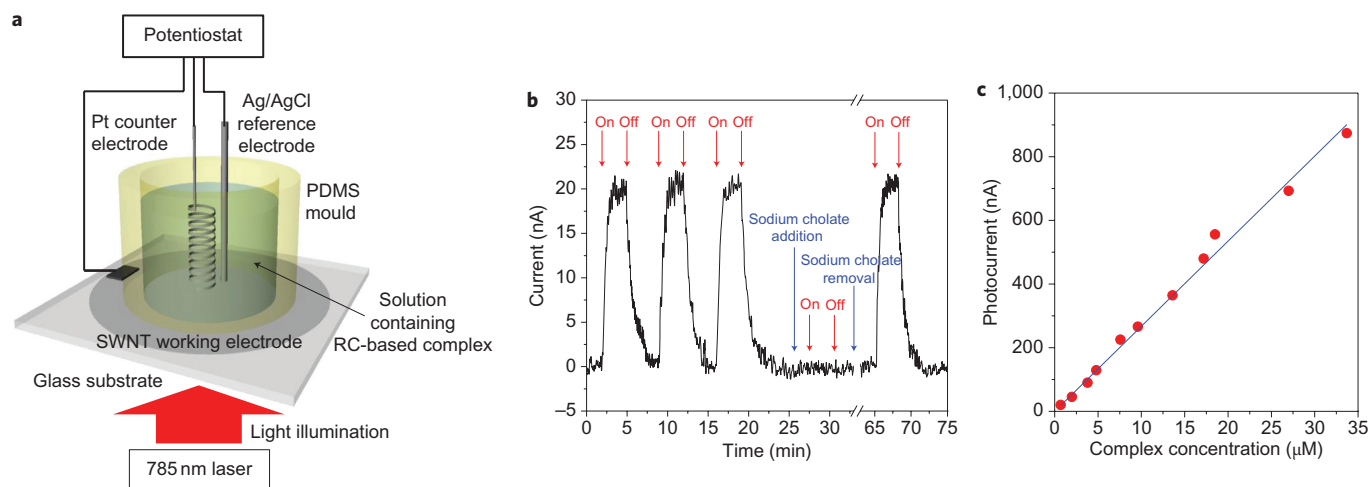
Figure 6 | Photoelectrochemical activity of an assembled RC–ND–SWNT complex in a photoelectrochemical cell. a, Schematic of the photoelectrochemical measurement apparatus, including a potentiostat in a three-electrode configuration. A transparent SWNT film cast on a glass substrate is used as the working electrode, and Ag/AgCl and coiled Pt wire as the reference and counter electrodes, respectively. A 785-nm laser diode illuminates the solution at 20 mW through an inverted microscope. **b,** Photoresponse of a 700 nM RC–ND–SWNT complex solution using 70 μM ferrocyanide and 70 μM ubiquinone as a double mediator in the photoelectrochemical cell. The photoelectrochemical activity disappears when the complex is broken apart by introducing sodium cholate, and is reinstated by reassembling the complex upon surfactant removal. **c,** Dependence of photocurrent on RC–ND–SWNT complex concentration ranging from 700 nM to 33.7 μM in the photoelectrochemical cell. The photocurrent increases linearly with complex concentration.

steps (Fig. 5; see also Supplementary Section S4). The surfactant removal rate controls the formation of ND–SWNT. There is a threshold rate of $\sim 1.0 \times 10^{-5} s^{-1}$, below which the system irreversibly forms pure lipid, protein and SWNT particulate phases. The system can only cycle reversibly between the metastable ND–SWNT and disassembled components by transitioning at a rate above this threshold. The magnitude of this limiting rate is fixed by the differences in kinetic timescales between the rapid ND–SWNT assembly process and the thermodynamically favoured, but kinetically slower, homogeneous phases.

Surprisingly, once formed, this dynamically assembled, purified RC–ND–SWNT complex has a photoelectrochemical activity that is present only in the assembled state (Fig. 6b). We monitored the photoresponse of the system using a double mediator scheme containing ferrocyanide/ferricyanide (70 μM) and ubiquinone/ubiquinol (70 μM) redox couples in a photoelectrochemical cell with a transparent bottom mounted on an inverted microscope (Fig. 6a). A SWNT film cast on a glass substrate was used as the transparent electrode[10,11] as it was found to produce a root mean square (r.m.s.) noise current of 1 nA, reduced by a factor of 50 compared with typical indium tin oxide (ITO) electrodes (Supplementary Fig. S8). A 700 nM RC–ND–SWNT solution in standard Tris buffer produces, under open-circuit conditions, a current that saturates at 20 nA and upon 20 mW laser illumination at 785 nm, as shown in Fig. 6b. This current of 20 nA translates into an external quantum efficiency of $8.0 \times 10^{-5}\%$ for a solution containing 8.4×10^{12} RC–ND–SWNT complexes (Supplementary Section S6). When the light is turned off, the current returns to the baseline.

In this reaction scheme, ferrocyanide either donates an electron directly to the P^+ site of the reaction centre or to the SWNT, which shuttles it to the photo-reduced P^+ site on the reaction centre $(P^+ + e^- \rightarrow P)$. The nanodisc assembly places this P site in close proximity to the nanotube. After electron transfer, ferricyanide travels to the working electrode, where it is reduced ($Fe(CN)_6^{3-} + e^- \rightarrow Fe(CN)_6^{4-}$). On the opposite side of the reaction centre, ubiquinone reduces to ubiquinol by accepting two electrons from the Q_A site in sequential turnovers of the reaction centre, shuttling the electrons to the anode[12–14]. Some interaction between the redox couples may also take place under these conditions[14]. The SWNT

acts primarily as a scaffold on which to collect $\sim$100 reaction centres in a single linear complex. The evidence shows that the photoresponse is substantially enhanced with this dual mediator system in the presence of SWNT when compared with the case of the ubiquinone mediator alone. The existence of a photoresponse in the presence of ubiquinone alone indicates that a process in which direct electron transfer to the P^+ site of the reaction centre is likely, but a detailed mechanism is under investigation (Supplementary Figs S11,S12, Supplementary Table S1).

As shown in Fig. 6c, the photocurrent increases linearly with increasing RC–ND–SWNT complex concentration. This implies that the photoresponsive output is limited by the number of photoactive complexes per volume. Embedding 10 mM of these complexes into a 1-μm-thick thin-film device would result in absorbance comparable to those exhibited by typical CdTe films with similar thicknesses (Supplementary Section S7)[15]. The requirement for such films is that the diffusion time of regeneration components must be shorter than the cycle time. Given that the largest diffusing component is the reaction centre, we calculate a minimum required diffusion time of 27 s for a 1-μm-thick film (Supplementary Section S7), which is significantly shorter than the 2-h cycle time allotted for reassembly of the complex. This motivates the exploration of thin-film geometries that use reaction centre-embedded matrices (Supplementary Fig. S14). Ongoing work in our laboratory is directed at exploring both re-concentrated colloidal cells and matrix materials that still allow for regeneration[16,17].

The complex enables the construction of a photoelectrochemical cell for which a regeneration cycle can be prompted using a chemical signal—sodium cholate addition or removal—alone. Figure 7a outlines a cell with two recirculating membrane dialysers, one 1,000 kDa and the other 12–14 kDa, for disassembly and reassembly, respectively. All components except the nanotube scaffold (damaged reaction centres, lipids and membrane scaffold proteins) can permeate the first dialyser when sodium cholate addition signals disassembly (Supplementary Fig. S13). The sodium cholate is then removed using the second dialyser, and the remaining lipids and proteins, supplemented from outside the loop, re-form the complexes. Without the regeneration cycle, the photocurrent falls off rapidly to 50% after 5 h and to 20%
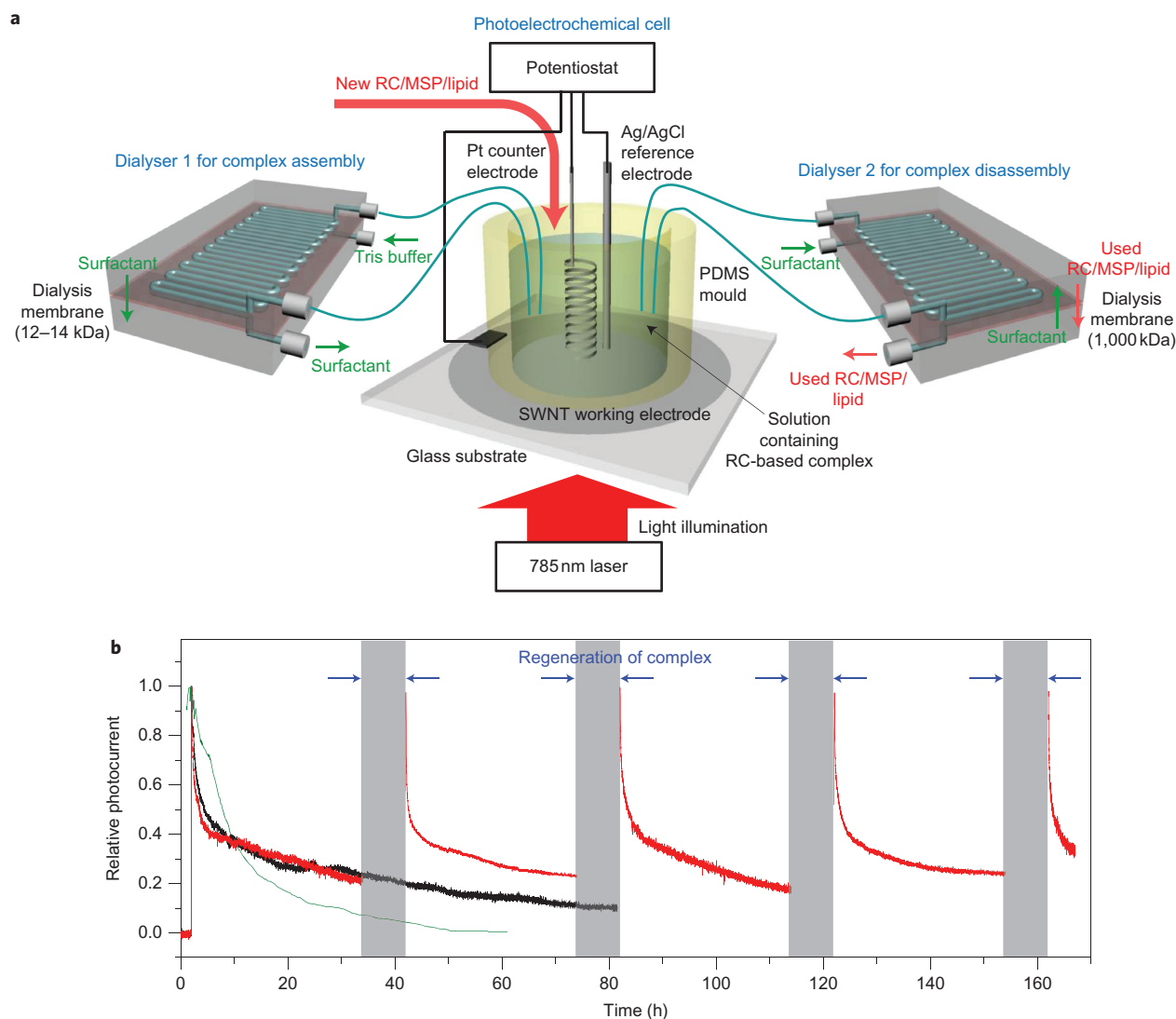
Figure 7 | Photoelectrochemical activity of a RC–ND–SWNT complex that autonomously regenerates. a, Schematic of the photoelectrochemical system, which comprises a photoelectrochemical cell incorporating two recirculating membrane dialysers. Dialysers 1 and 2 are used for assembly and disassembly of the complex with 12–14 kDa and 1,000 kDa pore membranes, respectively. The photo-damaged reaction centres, membrane scaffold proteins and lipids are removed during dialysis for disassembly of the complex and are replaced with new components, whereas the SWNTs are retained. The disappearance of reaction centre photoluminescence peaks after disassembly confirms the complete removal of photo-damaged reaction centres before reassembly (Supplementary Fig. S13). **b**, Temporal photoresponse of the RC–ND–SWNT with and without regeneration. Without regeneration (black curve), the photocurrent decreases sharply, falling to 50% after 5 h and 10% after 80 h. Deactivation is comparable to dye-sensitized solar cell (DSSC) data published in the literature (green curve)[21]. Operating the regeneration cycle every 32 h for a duration of 8 h restores the photocurrent to the previous maximum and extends the device lifetime indefinitely. Over 168 h, efficiency is increased by more than 300%.

after 32 h (Fig. 7b). Although some photoelectrochemical cells exhibit stability over 1,000 h (refs 18–20), many cells described in the literature have deactivation rate constants comparable to our unregenerated cell, as illustrated by recent measurements on quasi-solid-state dye-sensitized solar cells that showed deactivation to zero photocurrent after 60 h (ref. 21).

We find that, immediately following each regeneration cycle (initiated every 32 h), the photocurrent is restored to the previous maximum, followed by a similar deactivation curve. Repeated regeneration appears to extend the lifetime of the device for over 168 h (Fig. 7b), and increases the photoconversion efficiency by more than 300%. The increase is limited by the frequency of regeneration steps, which we arbitrarily set at 8.7×10^{-6} Hz, and the length of the regeneration cycle (8 h). More efficient dialysers and mass transfer, such as those encountered in a microfluidic platform, would shorten both times. In theory, the device could regenerate just as

easily from biological components derived from waste biomass[22–24], or by coupling directly to conventional biosynthesis in a manner similar to natural chloroplast operation[25–27].

In conclusion, we have demonstrated the first synthetic photoelectrochemical complex capable of chemically triggered disassembly and specifically orientated reassembly based solely upon intermolecular forces and thermodynamic equilibrium. This reversible assembly and disassembly process enables the synthesis of a photoelectrochemical cell that can autonomously regenerate using only a chemical signal (surfactant addition and removal). To date, only natural photosynthetic systems have shown the ability to disintegrate complex light-harvesting machinery that precisely reassembles after repair. By more closely mimicking such dynamic systems, we may be able to design more robust, fault-tolerant solar energy conversion schemes that approach the process that took Nature over 100 million years of evolution to develop.

Methods

Self-assembly through membrane dialysis. Nanodisc synthesis procedures are described elsewhere[4,8]. Briefly, DMPC (Avanti Polar Lipids) and Laurdan (6-dodecanoyl-2-dimethylaminonaphthalene, Molecular Probes) in chloroform were dried with high-purity N_2 and in a vacuum chamber before suspension in aqueous solution with 0.1 M sodium cholate. Membrane scaffold proteins were produced using a BioFLo 410 fermenter according to protocols described previously[4]. These membrane scaffold proteins are a class of amphiphatic proteins based on the apolipoprotein A-I sequence without the globular N-terminal domain that is present in the native proteins. The proteins were isolated using a Ni-affinity resin and the quality verified by electrospray mass spectrometry and SDS–polyacrylamide gel electrophoresis (SDS–PAGE). Membrane scaffold proteins were added to the solution at a molar ratio of DMPC:MSP:Laurdan of 100:1:1. As-prepared HiPco or CoMoCAT nanotubes were obtained from Rice University and Southwest Nanotechnologies, respectively. The reaction centres were isolated from R. sphaeroides and suspended in 0.1% LDAO and 0.1 M tris(hydroxymethy1)aminomethane hydrochloride (Tris–HCl) at pH 8.0 (refs 28,29). SWNTs, initially dispersed in deionized water with 2 wt% sodium cholate, and reaction centres were added to yield final concentrations of 4–20 mg l^{-1} and 0.003–33.7 μM, respectively. The mixture solutions were dialysed against the Tris buffer using 12–14 kDa pore membranes (Spectrum Laboratories). The buffer was replaced every 8 h, and self-assembled nanomaterials are collected after 24 h.

AFM and SANS. The self-assembled complexes were visualized with an AFM (Veeco Metrology) in contact mode. The complexes were placed on a mica surface in a fluid cell with imaging buffer (10 mM Tris (pH 8.0), 0.15 M NaCl and 10 mM $MgCl_2$). SANS experiments for the complexes were carried out on the 30-m NG7 beamline at the National Institute of Standards and Technology (NIST) Center for Neutron Research (NCNR) (Supplementary Section S1). All solutions were dialysed against D_2O before measurements to improve scattering contrast against the pure hydrogenated components.

Material purification using ultracentrifugation. The dialysed materials contained a mixture of self-assembled components, which were separated based on their density differences using an ultracentrifuge (Optima L-100 XP, Beckman Coulter), following a procedure developed by Arnold and colleagues[7]. Specifically, each dialysed sample was added onto a 5-ml stop layer (60% iodixanol, Optiprep, Sigma) in a centrifuge tube, followed by serial addition of 50, 40, 30, 20 and 10% gradient layers (1 ml each). After centrifugation at 30,000 r.p.m. for 7 h, a fraction recovery system (Beckman Coulter) was used to extract 250-μl aliquots from the centrifuge tube into each well of a 96-well plate with a programmed translational stage. The densities of fractionated portions were determined by measuring the mass of 100 μl of water from each well after ultracentrifugation and fractionation under the same conditions as other samples.

Spectroscopic characterization. Optical density was determined using a UV-vis-NIR spectrophotometer (UC-3101PC, Shimadzu). A plate reader (Varioskan Flash, Thermo Scientific) was used to measure optical absorption and Laurdan fluorescence from fractionated samples. The samples were also characterized with resonance Raman (Kaiser Optical Systems) and photoluminescence (PI Action) spectroscopy using a 785-nm laser diode (Ocean Optics) for excitation. The fluorescence of (9,1) nanotubes at ~925 nm was used to detect the presence of SWNTs because of the strong photoluminescence response. Steady-state photoluminescence excitation spectra were obtained with a home-built scanning spectrofluorometer equipped with a xenon lamp and a cryogenically cooled germanium detector. Increments of 10 and 4 nm were used in the excitation and emission monochromators.

Photoelectrochemical measurements. Photoelectrochemical properties were investigated with a potentiostat (Princeton Applied Research, 273A), a coiled platinum wire auxiliary counter electrode and an Ag/AgCl reference electrode (BASi). A transparent SWNT film cast on a glass substrate was used as the working electrode (Supplementary Section S5)[10,11]. The photoactive solution was contained within a PDMS (Sylgard 184, Dow Corning) mould with a cylindrical hole, which was clamped onto the glass substrate. This setup was mounted on the inverted microscope and illuminated with a 785-nm laser diode with an irradiance of 20 mW (Fig. 6a). To detect the photoelectrochemical response, 70 μM ferrocyanide ($K_4Fe(CN)_6$) and 70 μM ubiquinone-2 ($C_{19}H_{26}O_4$) were used as redox mediators in Tris buffer solution. The photoresponse of the system was measured under open-circuit conditions by turning on and off the light source. To examine the lifetime using regeneration, we devised a photoelectrochemical system consisting of a cell connected to two dialysers with membranes with 12–14 kDa and 1,000 kDa pores, for assembly and disassembly, respectively. Although the mixture solution flowed through the 12–14 kDa pore membrane, the complex self-assembled upon surfactant removal. After measuring photoelectrochemical activity for 32 h, the complex was dialysed for 6 h against the surfactant buffer using a 1,000 kDa pore membrane to disassemble the complex and subsequently remove used reaction centres, membrane scaffold proteins and lipids while retaining the SWNTs. The complex was reassembled upon surfactant removal for 2 h by adding new components, including reaction centres. This assembly–disassembly process was repeated throughout lifetime measurements.

References

1. Aro, E. M., Virgin, I. & Andersson, B. Photoinhibition of photosystem II. Inactivation, protein damage and turnover. *Biochim. Biophys. Acta—Bioenerg.* **1143,** 113–134 (1993).
2. Melis, A. Dynamics of photosynthetic membrane composition and function. *Biochim. Biophys. Acta—Bioenerg.* **1058,** 87–106 (1991).
3. Richard, C., Balavoine, F., Schultz, P., Ebbesen, T. W. & Mioskowski, C. Supramolecular self-assembly of lipid derivatives on carbon nanotubes. *Science* **300,** 775–778 (2003).
4. Bayburt, T. H., Grinkova, Y. V. & Sligar, S. G. Self-assembly of discoidal phospholipid bilayer nanoparticles with membrane scaffold proteins. *Nano Lett.* **2,** 853–856 (2002).
5. Jones, M. R. The petite purple photosynthetic powerpack. *Biochem. Soc. Trans.* **37,** 400–407 (2009).
6. Hoff, A. J. & Deisenhofer, J. Photophysics of photosynthesis. Structure and spectroscopy of reaction centers of purple bacteria. *Phys. Rep.—Rev. Sec. Phys. Lett.* **287,** 1–247 (1997).
7. Arnold, M. S., Green, A. A., Hulvat, J. F., Stupp, S. I. & Hersam, M. C. Sorting carbon nanotubes by electronic structure using density differentiation. *Nature Nanotech.* **1,** 60–65 (2006).
8. Denisov, I. G., McLean, M. A., Shaw, A. W., Grinkova, Y. V. & Sligar, S. G. Thermotropic phase transition in soluble nanoscale lipid bilayers. *J. Phys. Chem. B* **109,** 15580–15588 (2005).
9. Ponder, J. W. & Case, D. A. Force fields for protein simulation. *Adv. Protein Chem.* **66,** 27–85 (2003).
10. Hu, L., Hecht, D. S. & Gruner, G. Percolation in transparent and conducting carbon nanotube networks. *Nano Lett.* **4,** 2513–2517 (2004).
11. Ham, M. H., Kong, B. S., Kim, W. J., Jung, H. T. & Strano M. S. Unusually large Franz–Keldysh oscillations at ultraviolet wavelengths in single-walled carbon nanotubes. *Phys. Rev. Lett.* **102,** 047402 (2009).
12. Agostiano, A., Caselli, M., Cosma, P. & Monica, M. D. Electrochemical investigation of the interaction of different mediators with the photosynthetic reaction center from *Rhodobacter sphaeroides*. *Electrochim. Acta* **45,** 1821–1828 (2000).
13. Trammell, S. A., Spano, A., Price, R. & Lebedev, N. Effect of protein orientation on electron transfer between photosynthetic reaction centers and carbon electrodes. *Biosens. Bioelectron.* **21,** 1023–1028 (2006).
14. Trammell, S. A., Wang, L., Zullo, J. M., Shashidhar, R. & Lebedev, N. Orientated binding of photosynthetic reaction centers on gold using Ni-NTA self-assembled monolayers. *Biosens. Bioelectron.* **19,** 1649–1655 (2004).
15. Khairnar, U. P., Bhavsar, D. S., Vaidya, R. U. & Bhavsar, G. P. Optical properties of thermally evaporated cadmium telluride thin films. *Mater. Chem. Phys.* **80,** 421–427 (2003).
16. Zhao, J. *et al.* Photoelectrochemistry of photosynthetic reaction centers embedded in Al_2O_3 gel. *J. Photochem. Photobiol. A* **152,** 53–60 (2002).
17. Kalabina, N. A., Zaitsev, S. Y., Zubov, V. P., Lukashev, E. P. & Kononenko, A. A. Polymer ultrathin films with immobilized photosynthetic reaction center proteins. *Biochim. Biophys. Acta—Biomembr.* **1284,** 138–142 (1996).
18. Sommeling, P. M., Spath, M., Smit, H. J. P., Bakker, N. J. & Kroon, J. M. Long-term stability testing of dye-sensitized solar cells. *J. Photochem. Photobiol. A* **164,** 137–144 (2004).
19. Kuang, D. *et al.* Stable, high-efficiency ionic-liquid-based mesoscopic dye-sensitized solar cells. *Small* **3,** 2094–2102 (2007).
20. Wang, M. *et al.* Efficient and stable solid-state dye-sensitized solar cells based on a high-molar-extinction-coefficient sensitizer. *Small* **6,** 319–324 (2010).
21. Biancardo, M., West, K. & Krebs, F. C. Quasi-solid-state dye-sensitized solar cells: Pt and PEDOT:PSS counter electrodes applied to gel electrolyte assemblies. *J. Photochem. Photobiol. A* **187,** 395–401 (2007).
22. Kermasha, S., Khalyfa, A., Marsot, P., Alli, I. & Fournier, R. Biomass production, purification and characterization of chlorophyllase, from alga (*Phaeodactylum tricornutum*). *Biotechnol. Appl. Biochem.* **15,** 142–159 (1992).
23. Voronin, P. Y. *et al.* Chlorophyll index and annual photosynthetic carbon sequestering in *Sphagnum phytocenoses*. *Russ. J. Plant Physiol.* **44,** 23–29 (1997).
24. Melis, A., Neidhardt, J., Baroli, I. & Benemann, J. R. Maximizing photosynthetic productivity and light utilization in microalgae by minimizing the light-harvesting chlorophyll antenna size of the photosystems. In *BioHydrogen* (ed. Zaborsky, O. R.) 41–52 (Plenum Press, 1998).
25. Dawson, T. L. Biosynthesis and synthesis of natural colours. *Color. Technol.* **125,** 61–73 (2009).
26. Moser, S., Muller, T., Oberhuber, M. & Krautler, B. Chlorophyll catabolites—chemical and structural footprints of a fascinating biological phenomenon. *Eur. J. Org. Chem.* **2009,** 21–31 (2009).
27. Vasilikiotis, C. & Melis, A. The role of chloroplast-encoded protein biosynthesis on the rate of D1 protein degradation in *Dunaliella salina*. *Photosynth. Res.* **45,** 147–155 (1995).

28. Goldsmith, J. O. & Boxer, S. G. Rapid isolation of bacteria photosynthetic reaction centers with an engineered poly-histidine tag. *Biochim. Biophys. Acta—Bioenerg.* **1276,** 171–175 (1996).
29. Takahashi, E. & Wraight, C. A. Proton and electron transfer in the acceptor quinone complex of *Rhodobacter sphaeroides* reaction centers: characterization of site-directed mutants of the two ionizable residues, GluL212 and AspL213, in the QB binding site. *Biochemistry* **31,** 855–866 (1992).

Author contributions

M.H.H., J.H.C., A.A.B. and M.S.S. designed the research. M.H.H., J.H.C., A.A.B., R.A.G. and D.A.H. synthesized the complexes. M.H.H. performed the photoelectrochemical experiments. J.H.C. purified the complexes and performed the spectroscopic experiments with A.C.C. A.A.B. performed kinetic modelling of complex formation. E.S.J. performed modelling of the DMPC configuration on the SWNT. A.M. and C.A.W. supplied the photosynthetic reaction centres. Y.V.G. and S.G.S. supplied the membrane scaffold proteins and conducted initial reconstitution experiments. T.H.B., A.S.Z. and K.J.V. performed AFM measurements. E.K.H. performed SANS measurements. M.S.S. originated the concept for the paper. M.H.H., J.H.C., A.A.B. and M.S.S. co-wrote the manuscript with input from S.G.S. and C.A.W.

Additional information

The authors declare no competing financial interests. Supplementary information accompanies this paper at www.nature.com/naturechemistry. Reprints and permission information is available online at http://npg.nature.com/reprintsandpermissions/. Correspondence and requests for materials should be addressed to M.S.S.